

Comparison of Superconducting NISQ Architectures

Benjamin Rempfer

Lincoln Laboratory

Massachusetts Institute of Technology

Lexington, MA USA

Benjamin.Rempfer@ll.mit.edu

Kevin M. Obenland

Lincoln Laboratory

Massachusetts Institute of Technology

Lexington, MA USA

Kevin.Obenland@ll.mit.edu

Abstract—Advances in quantum hardware have begun the noisy intermediate-scale quantum (NISQ) computing era. A pressing question is: what architectures are best suited to take advantage of this new regime of quantum machines? We study various superconducting architectures including Google’s Sycamore, IBM’s Heavy-Hex, Rigetti’s Aspen and Ankaa in addition to a proposed architecture we call bus next-nearest neighbor (busNNN). We evaluate these architectures using benchmarks based on the quantum approximate optimization algorithm (QAOA) which can solve certain quadratic unconstrained binary optimization (QUBO) problems. We also study compilation tools that target these architectures, which use either general heuristic or deterministic methods to map circuits onto a target topology defined by an architecture.

Index Terms—quantum architectures, qubit connectivity, compilation, qubit routing, circuit scheduling, superconducting qubit, 2-local Hamiltonian, QAOA, NISQ

I. INTRODUCTION

Many commercial and government entities are placing significant emphasis on the research and development of quantum computers. Machines available today are deemed Noisy Intermediate Scale Quantum (NISQ) as a reference to the fact that they are both noisy and modest in scale. Much research pertaining to benchmarking and demonstrating quantum devices today is limited to small-scale architectures with a few qubits. This research is critical to reducing noise and producing higher fidelity qubits [1], but it does not address issues related to the design of future architectures. Only recently have companies begun to run experiments with dozens or even a hundred qubits [2] [3]. We aim to address the problem of which architectures are best suited to take full advantage of precisely this intermediate scale of dozens of qubits and beyond. This paper restricts its focus to superconducting devices implementing circuits without error correction. There are a multitude

of considerations that must be made when comparing NISQ superconducting architectures. In order to fully understand the design space we introduce some preliminary definitions and nomenclature typically associated with superconducting quantum devices.

Superconducting devices have a predefined set of quantum gates, called its gateset, which can be executed natively within a set amount of time (referred to as the gate’s runtime). Quantum circuits are commonly written as an ordered set of instructions (gates) that allow arbitrary single-qubit gates $g_1 \in SU(2)$ as well as entangling gates between arbitrary pairs of qubits $g_2 \in SU(4)/SU(2) \otimes SU(2) \simeq SO(4)$. Real devices cannot enact arbitrary entanglement in this way. Thus, we define the set of pairs of qubits on which entangling interactions are executable on some quantum device as its coupling map (sometimes called its topology). Together, a quantum computer’s topology and gateset define its *architecture*. Running a quantum circuit on a specific superconducting architecture requires translating the base circuit to a different quantum circuit (that represents the same unitary) so as to adhere to the restrictions of a specific device.

The process of translating a quantum circuit to run on a specific architecture is known as compiling. Finding an optimal compilation solution is NP-hard [4], and thus heuristic techniques are typically employed. Note that we do not consider the lower-level problem of translating quantum gates into sequences of microwave pulses (together with compiling called transpiling). Various heuristics and some limited exact methods exist to tackle the compilation problem for general quantum circuits. For this reason, resource analysis of algorithms applied to various device architectures is important when developing new quantum algorithms or considering the implementation of existing algorithms. To this end, two prominent metrics for comparing quantum algorithms compiled to separate architectures are entangling (typically two-qubit) gate count and circuit depth. Two-qubit gate count is an important metric because these gates are typically the lowest fidelity. The circuit depth m is the number of sequential layers of gates in the total circuit. Single-qubit gates are often neglected in depth calculations as they can be executed in parallel across separate qubits and take less time to execute than entangling gates. The depth of a given circuit can be found as the longest path in the directed acyclic dependency graph it generates. Reducing the number of two-qubits gates and the depth of the circuit

DISTRIBUTION STATEMENT A. Approved for public release. Distribution is unlimited.

This material is based upon work supported by the Under Secretary of Defense for Research and Engineering under Air Force Contract No. FA8702-15-D-0001. Any opinions, findings, conclusions or recommendations expressed in this material are those of the author(s) and do not necessarily reflect the views of the Under Secretary of Defense for Research and Engineering.

©2024 Massachusetts Institute of Technology.

Delivered to the U.S. Government with Unlimited Rights, as defined in DFARS Part 252.227-7013 or 7014 (Feb 2014). Notwithstanding any copyright notice, U.S. Government rights in this work are defined by DFARS 252.227-7013 or DFARS 252.227-7014 as detailed above. Use of this work other than as specifically authorized by the U.S. Government may violate any copyrights that exist in this work.

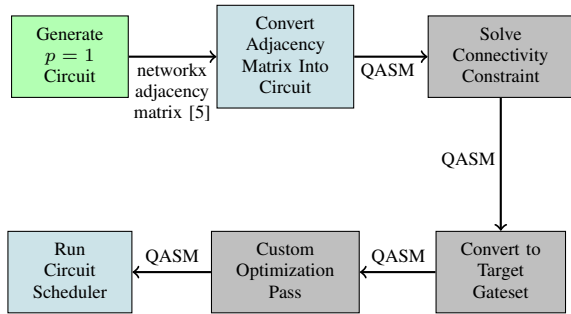


Fig. 1. Flowchart showing how a problem instance and architecture are used to produce a compiled circuit which is then converted into a benchmarkable metric. From the final scheduled circuit we extract our chosen metrics.

both have a direct impact on the fidelity and execution time of the circuit.

It is worth noting that while depth can be a useful metric, a better measure of the performance of a circuit is *scheduled time*. The scheduled time of a quantum circuit, on a given quantum computer, is the summation a circuit’s critical path weighted with each gate’s runtime. A circuit’s critical path is the longest ordered set of gates that cannot be run in parallel on a specific quantum computer. For most architectures this corresponds directly to a circuit’s depth, where qubits represent the only dependency in the machine. However, this is not always the case; machines could contain components (such as a bus described in Section II) that impose additional structural dependencies on the execution of gates. Differences in runtime and gateset can further distance a circuit’s scheduled time from its depth.

Clearly, there are numerous trade-offs and a large design space to consider in analyzing near-term quantum architectures. In order to accurately compare NISQ devices one must take coupling maps, gatesets, compiling tools, and quantum algorithms into account. This study has two main contributions to present. The first is an evaluation of current and proposed superconducting qubit architectures. The second is a comparison of a representative set of compilation tools and techniques. In Figure (1) we illustrate the compilation process used in our work. We start with a problem instance and a definition of the device architecture. The problem is then compiled to the architecture, which gives a circuit that can be analyzed to determine the scheduled time and two-qubit gate count. All circuits are treated with the same custom optimization pass as to control for differences in commercial implementations.

The structure of the paper is as follows; we first describe various existing coupling maps in section (II). In Section (III) we detail the specific adjacency matrices that specify the Quantum Approximate Optimization Algorithm (QAOA) benchmark circuits. In Section (IV), we give a number of compilation tools that we use and compare. We present the results of our study in Section (V) and finally conclude and discuss future research in Section (VI).

II. SUPERCONDUCTING QUBIT TOPOLOGIES

A. Planar

There are a number of similar, but distinct, superconducting quantum device architectures in development. The three main commercial architectures that we will focus on are Google’s Sycamore, Rigetti’s Aspen, and IBM’s heavy-hex. At the time of writing, the largest publicly announced Google chip is Bristlecone which contains 72 qubits in a grid-like configuration. Rigetti’s 3rd generation chip uses the Aspen architecture consisting of four octagons with qubits at each vertex positioned in a 4×2 grid with two connections between adjacent octagons for a total of 80 qubits. Recently, Rigetti announced that subsequent generations will no longer utilize this device architecture and instead employ a 2D grid and be called Ankaa [6]. Finally, IBM devices are defined on a “heavy-hex” architecture [7]. The largest IBM device deployed on the cloud today is 133 qubits with announcements promising many more. Heavy-hex is made up of tiled hexagons with qubits occupying each vertex and side. For completeness, we also include two generic coupling maps in our analysis: a one-dimensional line and a two-dimensional grid (similar to Rigetti’s announced system). A depiction of the three main planar architectures is shown in Figure (2).

The connectivity of a topology is defined as the average number of edges per node. All commercial architectures are planar graphs with average connectivities ranging from ≈ 2.27 for IBM Eagle to ≈ 3.36 for Google Bristlecone. Intuitively, higher connectivity leads to lower depth circuits. However, the amount of parallelism present in the circuit will have an impact on the performance. As will be discussed in Section (IV), in general, a logarithmic depth overhead $\Omega(\log n)$ is necessarily incurred when utilizing coupling maps with finite degree [4]. However, this overhead is only theoretically achievable. In practice, this lower-bound is difficult to reach.

B. Non-Planar

In addition to the planar coupling maps defined above, we introduce two architectures based on non-planar coupling maps (see Figure (3) for an illustration of these two architectures). These non-planar graphs gain connectivity but are more complex to fabricate than the planar topologies. First is the layered Sycamore chip, which is defined as two Sycamore chips connected via transverse vertical links. This increases the average number of edges per qubit from ≈ 3.36 to ≈ 4.36 .

Our final coupling map utilizes a (qubit) *bus* [8] [9]. This bus allows arbitrary two-qubit gates between any pair of qubits connected to it. However, each entangling gate must be sequentialized. The bus increases connectivity but comes with the trade off of added hardware complexity and reduced parallelism. There is a natural optimization between the number of qubits connected via a bus $|B|$ and the total number of buses B . Larger buses reduce the number of swaps required but also reduce the parallelism of a circuit. Our base-line design utilizes buses with $|B| = 8$ qubits, which are connected via point-to-point connections (an architecture

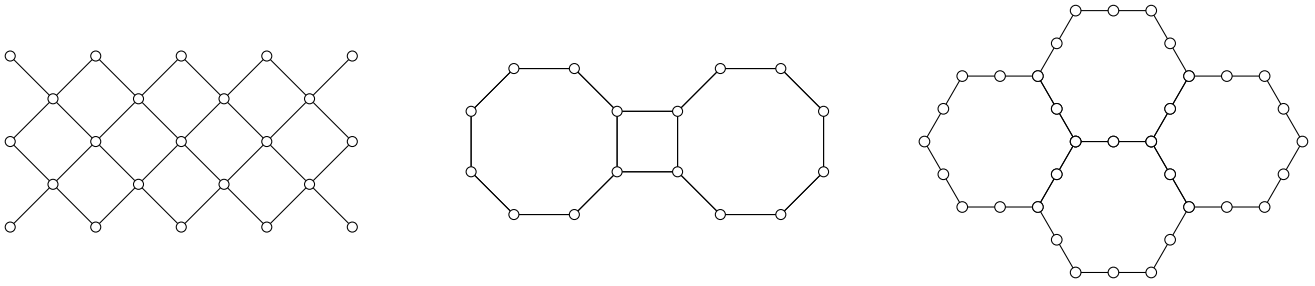


Fig. 2. Commercially available architectures. From left to right: a 23 qubit example of Google’s Sycamore architecture, a 16 qubit subgraph of a Rigetti Aspen chip, and four tiled heavy-hexagons illustrating IBM’s architectures.

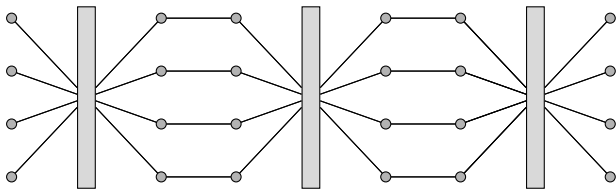
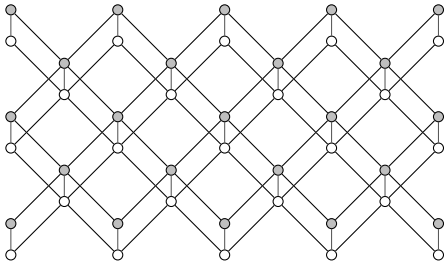


Fig. 3. A layered configuration of 23 qubit sycamore chips (top) and a graphical representation of the busNNN topology (bottom). In the busNNN architecture, each rectangle represents a bus that can be dynamically reconfigured to connect any pair of qubits connected to it. The number of qubits connected to a bus is a parameter of the bus definition, and we assume that a bus can only execute a single two-qubit gate at a time (although this could conceivably be altered).

we call bus next-nearest neighbor (busNNN) as illustrated in Figure (3). These architectures are listed in Table (I).

III. QAOA PROBLEM INSTANCES

In our study of superconducting architectures, it is important to benchmark relevant quantum algorithms. One such algorithm is the Quantum Approximate Optimization Algorithm (QAOA) which is itself a 2-local Hamiltonian simulation. Its circuit thus has qualitatively similar structure to other important quantum algorithms including Hamiltonian simulation for Heisenberg, XY, Ising, and Fermi-Hubbard models [10] [11] [12].

QAOA produces approximate solutions for combinatorial optimization problems [13] [14] [15]. These problems are

specified by minimizing an objective function

$$C(z) = \sum_{ij} A_{ij} z_i z_j$$

over $z \in \{\pm 1\}^N$ where $A \in \mathcal{M}(\mathbb{R})_{N \times N}$ is the adjacency matrix for the problem instance encoded as an undirected weighted graph [16]. The quantum circuit consists of $p \in \mathbb{Z}^+$ layers with classical processing sandwiching each. In the version of QAOA solving maxcut, all layers consist of the parameterized unitary

$$U(\beta, \gamma) = \prod \exp(i\gamma ZZ) \prod \exp(i\beta X)$$

where $\gamma, \beta \in \mathbb{R}$ are the angles to be classically optimized and change from layer to layer. In the limit $p \rightarrow \infty$, QAOA converges to an optimal solution. As every layer is identical, we consider $p = 1$ QAOA max-cut circuits for simplicity. It is an active area of research to determine the value of p where QAOA yields quantum advantage in terms of speed and/or solution quality. Near-term devices can only run relatively-low depth circuits and thus stand firmly in the low- p regime [17] [18]. Note that, for the subsequent discussion of problem instance candidates, the weights in each graph contribute nothing to our desired metrics related to compilation and can therefore be ignored. Our study is not of the performance of QAOA, but rather the scheduling and compilation of circuits to target coupling maps, for which we choose QAOA to be representative of 2-local Hamiltonian simulation circuits. We explicitly employ QAOA for max-cut circuits because their qualitative structure is similar to 2-local Hamiltonian simulation circuits and they are straightforward to generate.

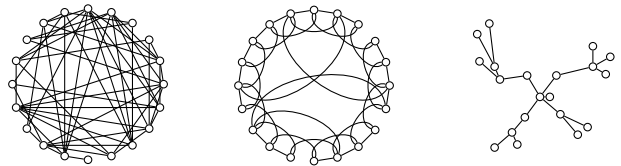


Fig. 4. On the left is an Erdős Rényi graph with $D \approx 1/2$. The center and right depict a Watts-Strogatz and Barabási-Albert graph respectively all with 20 vertices.

As alluded to above, 2-local Hamiltonian simulation algorithms are naturally described by an adjacency matrix, with nodes corresponding to variables (qubits) and edges corresponding to terms in the Hamiltonian. There are a number

All Considered Coupling Maps				
Topology	Qubits	Connectivity	Type	Existence
Sycamore	72	≈ 3.36	Planar	Commercial
Aspen	80	2.5	Planar	Commercial
Eagle (heavy-hex)	127	≈ 2.27	Planar	Commercial
Line	n	$2(n-1)/n$	Planar	Hypothetical
2D Grid	N^2	$4(N-1)/N$	Planar	Hypothetical
Layered	144	≈ 4.36	Non-Planar	Hypothetical
busNNN	B	$ B (B -1)/2$	Non-Planar	Hypothetical

TABLE I
COUPLING MAPS FOR THE ARCHITECTURES CONSIDERED IN THIS STUDY. THE SIZE OF EACH DEVICE INSTANCE IS EITHER FIXED OR VARIED TO ACCOMMODATE THE NUMBER OF QUBITS IN A CIRCUIT.

All Considered Problem Instances		
Model Graph	Description	Applications
3 regular	degree 3	maxcut
12 regular	degree 12	maxcut
Watts-Strogatz (WS)	high clustering	small-world, community structure, etc.
Barabási-Albert (BA)	power law growth	social networks, price models, etc.
Sherrington-Kirkpatrick (SK)	fully connected	Ising and spin-glass
Erdős Rényi (ER)	“average” graph	unstructured problems

TABLE II
GRAPH TYPES CONSIDERED IN THIS STUDY. THE ANALYSIS IS PERFORMED USING $p = 1$ QAOA IMPLEMENTATIONS.

of choices for graphs to be used as a problem instances including random Erdős-Rényi (ER) graphs. The ER model selects a graph with N nodes and M edges by choosing from all possible graphs with density $D = 2M/N(N+1)$ uniformly at random. We can define multiple unique graphs, leading to unique QAOA circuits, of a given density.

Random graphs, however, may be qualitatively different from graphs corresponding to real problem instances. Therefore we must expand our search to other types of graphs that are perhaps more explicitly linked to real problems in combinatorial optimization. We turn to connected 3-regular and 12-regular graphs with unit weight. Random regular graphs are given by placing edges between vertices until every vertex is connected to the specified number of other vertices, in this case 3 or 12. We also consider completely-connected Sherrington Kirkpatrick (SK) graphs. This is a specific case of ER graphs with $D = 1$. It provides a useful benchmark for the most dense graphs possible. SK graphs can be used to define a type of spin-glass model.

The final two problem instances we use are Watts-Strogatz (WS) and Barabási-Albert (BA) graphs. WS graphs improve the clustering of ER graphs. ER graphs do not generate local clustering or triadic closures (they possess a low clustering coefficient). WS graphs account for clustering while retaining short path lengths. A WS graph is constructed by starting with a ring graph and adding $k = 4$ next-nearest neighboring connections. Then one rewires edge ij to ik with probability $p = 1/2$. BA graphs address another key shortcoming of the ER model: the scaling of degree. The degree distribution of ER graphs converges to the Poisson distribution, as opposed to the power law which is more realistic. These graphs are built by starting with a star graph with $\lceil n/4 + 1 \rceil$ nodes. Then an additional $\lceil 3n/4 - 1 \rceil$ nodes with $\lceil n/4 \rceil$ edges are attached

to higher degree existing nodes.

We illustrate ER, WS, and BA graphs in Figure (4). In Table (II) we summarize the graph types used to create benchmark circuits in our study.

IV. COMPILING TOOLS

A. Heuristic

Similar to Section (II) detailing the many existing commercial coupling maps, there are a comparable number of compiling tools. The hardware and algorithm agnostic heuristics we consider are IBM’s implementation of SwAp-based Bidirectional search (SABRE) [19] and the router provided by Tket [20]. In addition to these general-purpose tools we consider an algorithmic-specific tool called 2QAN, which takes advantage of the structure of 2-local Hamiltonian’s for further optimization not possible in the tools based on general heuristics [21].

The first heuristic compiling tool, SwAp-based BiDiRectional search (SABRE), utilizes a directed acyclic graph representation of the quantum circuit. It is based on two main design principles: prioritizing gates with near-term dependencies, and the novel idea of traversing the reversed circuit to find an initial mapping. (Finding a good initial mapping is a nontrivial component of compilation.) Tket’s router uses a time-sliced version of a circuit to construct an initial mapping. In both heuristics a distance measure is used as a cost function. Afterwards, we utilize some of qiskit’s optimization passes to clean up any unwanted artifacts of compilation [22].

SABRE and Tket’s heuristic algorithms are powerful. However, they operate at the gate level and therefore cannot take advantage of structural properties of the algorithm. The ability to optimize at the operator-level allows for additional resource reductions. In QAOA it is obvious to see that all

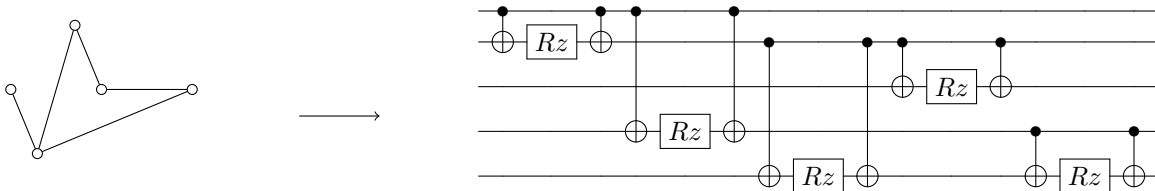


Fig. 5. On the left is an example problem instance graph. The right depicts a subcircuit of a QAOA instance on 5 qubits corresponding to that example problem instance. $\text{Exp}(i\theta ZZ)$ operators can be permuted to reduce the depth of the circuit from 5 time steps to 3. In general, a 2-local Hamiltonian’s operators may not commute but can still be arbitrarily permuted.

All Considered Compilers		
Compiler	Description	Provider
SABRE	traverses DAG twice	IBM
Tket	time slices circuit	Quantinuum
2QAN	Tabu search	open source
shuffle	low computational overhead	internal implementation

TABLE III

ALL COMPILING TOOLS CONSIDERED IN THIS STUDY. THESE TOOLS PROVIDE A REPRESENTATIVE SAMPLE OF CURRENTLY AVAILABLE TOOLS.

entangling operators commute and therefore reordering at the operator level results in significant improvements to the compilation solution. It is also the case, however, that any 2-local Hamiltonian can be reformulated with effectively commuted entangling operations. This potential optimization is completely invisible to SABRE and Tket. In Figure (5) we show a circuit that can be reduced in depth by 2QAN, but not by the other tools.

In other words, there are N_A distinct adjacency matrices for the same problem graph G where

$$N_A = \frac{n!}{|\text{Aut}(G)|}$$

and $\text{Aut}(G)$ is the group of functions preserving the group structure of G [23]. The quantum circuits generated from these different matrices will be represented via distinct unitaries and are thus inaccessible to the gate-level optimization present in many commercial compilers. 2QAN takes advantage of this added optimization space via a Tabu search [24] at the expense of compilation runtime.

B. Deterministic

One crucial drawback, with these heuristic algorithms, is that their runtime scales poorly at large problem sizes. Deterministic routing algorithms, on the other hand, can compile very large circuits with predictable, low constant factor scaling. One such algorithm is the full-shuffle which was independently developed by Jin et. al. (called Multi-dimensional All-to-All Permutation and Swaps MAAPS) [25] and IBM (implemented in commutative SABRE) [26]. These techniques provide scalability to larger system sizes when one has access to patterned coupling maps. The line and 2D grid strategies have been worked out in the papers above. This allows us to formalize the runtime of shuffle networks, which we restate for completeness in the following theorems.

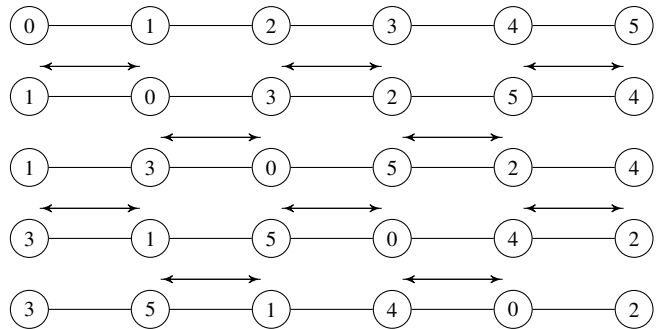


Fig. 6. A fully shuffled line topology with $n = 6$ component qubits. Each row depicts a swap reconfiguration step, with time flowing from top to bottom.

Theorem 1. *For the line graph of size n , the swap strategy that alternates between two swap layers, one on all odd numbered edges, and one on all even numbered edges reaches full connectivity in $n - 2$ layers and is optimal.*

The proof is given in the references above and intuition is illustrated in Figure (6). Note that a provably optimal full shuffle strategy for a 2D grid has not yet been discovered. Still, a swap strategy has been developed; its proof is also contained in the above references. The two-dimensional strategy alternates between applying $N - 1$ steps of the line swap strategy to each row individually and swapping all rows by applying exactly two steps of the line swap strategy to each column. The code given in Figure (7) shows how to generate those layers and store them in the dictionary swaps with keys corresponding to each layer index. We develop an analogous full shuffle strategy for our proposed busNNN architecture. The design of this architecture is motivated by the optimality of its swap strategy, however it is still prudent to test its performance with other compilation algorithms.

Theorem 2. *For the 2D grid of size $n = N^2$ the swap strategy of alternating $N - 1$ steps of the line swap strategy to each row and swapping rows in parallel reaches full connectivity in no more than $\frac{1}{2}(N - 2)(N + 1)$ layers.*

Theorem 3. *For the busNNN architecture with B buses the swap strategy that alternates between two swap layers, one between adjacent half columns not contained within the same bus, and one between half columns on the same bus except the B -th bus, reaches full connectivity in precisely $(4B - 5)\lceil \frac{B}{B+1} \rceil$ layers.*

```

for row in range(N):
    for col in range(row*N, row*(N+1)):
        if (((col%N)%2)==0 and ((col%N) != (N-1))):
            if (row%2==0):
                swaps[0].append((col, col+1))
            if (row%2!=0):
                swaps[1].append((col, col+1))
        if (((col%N)%2)!=0 and ((col%N) != (N-1))):
            if (row%2==0):
                swaps[1].append((col, col+1))
            if (row%2!=0):
                swaps[0].append((col, col+1))
for col in range(N):
    for row in range(N):
        if (((row+col*N)%N)%2)==0):
            if ((col+row*N+N) <= (N**2-1)):
                swaps[2].append((col+row*N, col+row*N+N))
        if (((row+col*N)%N)%2)!=0):
            if ((col+row*N+N) <= (N**2-1)):
                swaps[3].append((col+row*N, col+row*N+N))

```

Fig. 7. Python code to generate the swap layers (stored in a dictionary of lists of pairs) needed for a full shuffle of some $N \times N$ 2D grid architecture.

Proof. Without loss of generality label the i -th half bus at time t' as $C(i, t')$ where indexing begins at 0 and t' is evolved by each swap layer. Denote half the qubits connected to a bus as a column and note that each column contains $|B|/2$ qubits. Following the initial swap layer,

$$C(i+1, 1) = \begin{cases} C(i, 0) + 1 & \dots (i \neq 2B - 1) \wedge (i \text{ even}) \\ C(i, 0) - 1 & \dots (i \neq 2B - 1) \wedge (i \text{ odd}) \\ C(i, 0) & \dots i = 2B - 1 \end{cases}$$

Clearly no duplicate combinations of columns have occurred within a bus when comparing $t' = 0$ and $t' = 1$. This is not the case when comparing $t' > 0$ odd and even. However, we can see that skipping every other time step yields a distinct set of pairs of columns aboard each bus. The sequence of columns that arrive at the 0-th index at time $t = 2t' - 1$ with $t' > 0$ is given by,

$$C(0, t) = \begin{cases} C(0, 2(t-1)) & \dots t \leq B \\ C(0, 2(2B-t) - 1) & \dots B < t < 2B \end{cases}$$

We can see that no spatially adjacent columns repeat at any moment in time when attached to the same bus by observing every $C(i, t)$ being identical across indices i up to a phase of exactly one reverse time step. Since these sequences are cyclic they will repeat after $2B - 1$ time steps. This, along with the initial mapping, ensures full connectivity between columns, and by extension qubits, is reached in $2B$ time steps. Transforming back to time being the number of swap layers we see full connectivity is reached in $4B - 5$ layers. Still, the case of one bus requires no swaps so we insert a factor of

$$\left[\frac{B}{B+1} \right] = \begin{cases} 0 & \dots B = 1 \\ 1 & \dots B > 1 \end{cases}$$

which gives the desired result. Code is given to generate this swap strategy in Figure (8). \square

```

if B > 1:
    for bus in range(1, B):
        for qbit in range(|B|/2 * (2*bus-1), |B|*bus):
            swaps[1].append([qbit-|B|/2, qbit])
swaps[0] = [swap for swap in interbus_connections]

```

Fig. 8. Python code to generate the swap layers (stored in a dictionary of lists of pairs) needed for a full shuffle of our busNNN architecture.

Corollary 1. *The swap strategy for busNNN is optimal in terms of number of swap layers required to reach full connectivity.*

For completeness, we now address the scaling of each coupling map's required number of swaps to reach full connectivity. The line strategy requires

$$L_{SWAP} = \frac{1}{2}(n-1)(n-2).$$

The $N \times N$ 2D grid requires a maximum of

$$G_{SWAP} = \begin{cases} \lceil \sqrt{N} \rceil (\lceil \sqrt{N} \rceil + 1) \left\lceil \frac{\lceil \sqrt{N} \rceil}{2} \right\rceil \left\lceil \frac{2\lceil \sqrt{N} \rceil - 3}{4} \right\rceil \dots \lceil N \rceil^{\text{odd}} \\ \left(\left\lceil \frac{\sqrt{N}}{2} \right\rceil (\lceil \sqrt{N} \rceil + 1)^2 + 2\lceil \sqrt{N} \rceil \left\lceil \frac{2\lceil \sqrt{N} \rceil - 3}{4} \right\rceil \right) \left\lceil \frac{\sqrt{N}}{2} \right\rceil \dots \text{else} \end{cases}$$

Finally, the busNNN topology requires

$$B_{SWAP} = \frac{|B|}{2} \left\lceil \frac{n-|B|}{|B|} \right\rceil \left(\frac{|B|}{2} \left\lceil \frac{n-|B|}{|B|} \right\rceil - 1 \right).$$

The scaling of these swap counts has a direct impact on the number of entangling gates. However, their relation to the depth is more clear in the number of layers as mentioned in theorems (1 – 3). Note that there are instances where optimization can still be applied to lower this overhead. Such a case is when the entangling gateset contains a sole CNOT gate. Then, in the busNNN architecture, one can match swap gates and entangling gates operating on the same qubits to reduce the total number of two-qubit gates used for the combined operation [27]. It is worth reiterating just how important deterministic algorithms, like the full shuffle, can be. They are easy to compute and thus scale better than heuristic algorithms at larger problem sizes. This transition from heuristic dominance to breakdown may well be within the range of NISQ devices. The main question we should then address is at what regime does this transition occur?

V. EXPLORING THE DESIGN SPACE

In this section we present the main results. We first compare all available compilers for a set of problem instances with the same coupling maps. We will utilize the number of entangling gates and scaled scheduled time as our metrics. Scaled scheduled time is the scheduled time when a single qubit gate takes 1 unit of time and an entangling gate takes 10. As mentioned before, we compile to the gateset of CNOT plus X and Z single qubit rotations. This is to ensure we are comparing compilers and coupling maps and not the idiosyncrasies of the gatesets of particular architectures. Because our random graphs result in

different adjacency matrices, we generate 100 graph instances for each configuration. Each circuit is compiled on a single Xeon-p8 processor maintained by the MIT LLSC team [28]. The “baseline” plot represents a fully connected architecture requiring no swaps or compiling passes.

In Figure (9), we see that although 2QAN does better in all cases with respect to the number of two-qubit gates. Although, the margin of that difference varies significantly. While shuffle’s scaling is deterministic, it cannot compete with any heuristic when applied to a sparse graph such as 3REG. As system size increases the density of regular graphs decreases via the relation $D = d/(n - 1)$ where d is the degree of regularity. We can then make some qualitative assertions on the performance of the given compilation tools. *Shuffle becomes better than 2QAN with larger and denser problem instances.* Using scheduled time as a metric yields significantly different results. While the above italicized statement is still true, the threshold where shuffle performs better than all heuristics is within the demonstrated data: convincingly within the NISQ regime. Broadly, SABRE performs better than Tket and takes significantly less compute time to run.

In Figure (10), we give the compile time for each tool for the compilation of a 12REG graph. When applied to larger and denser graphs, 2QAN can take days or even weeks of compute time to compile a single circuit. When the actual scheduled time of these quantum circuits would be on the order of microseconds, this scaling is unacceptable. This is why shuffle was proposed. Nonetheless, while there is a scaling guarantee of the full shuffle method it does not ever reach the desired logarithmic overhead in any practical setting.

Aside from taking weeks to compile a single circuit, scaling to larger problem sizes does not have much of an effect on the qualitative behavior we observe at smaller problem instances. One meaningful difference is that SABRE seems to do worse for larger and denser circuits. Along that same vein, we can see that shuffle does become better than both Tket and SABRE past some threshold, as conjectured above. This happens at larger densities for more connected architectures. This fits with the scaling we derived in Section (IV). It is clear that 2QAN consistently outperforms other heuristics as it is taking advantage of optimization invisible to the other compiling methods. So far, we have only discussed hypothetical architectures. The three commercial architectures introduced in Section (III) were Google’s Sycamore, IBM’s heavyhex, and Rigetti’s Aspen. We do not derive the swap layers required to apply the shuffle compilation method to these topologies. One simple strategy could be to unwind Rigetti’s Aspen and IBM’s heavyhex architectures into a line and apply the line swap strategy (with slight correction terms in heavyhex’ case). A slightly modified version of the 2D grid swap strategy could be applied to Google’s Sycamore. Nonetheless, the three heuristic algorithms’ data is compared in Table (IV). The layered Sycamore chip is also included.

We now turn to the performance of the circuits utilizing the different coupling maps. In Figure (12) we show a comparison across the different architectures. A few striking observations

Google’s Sycamore				
<i>Entangling Gates</i>	18q	36q	54q	72q
SABRE	174±13	460±32	833±44	1286±69
Tket	179±14	489±34	884±55	1435±84
2QAN	133±13	349±27	614±43	966±56
<i>Scaled Sched Time</i>				
SABRE	944±134	1827±260	2838±339	3991±509
Tket	1124±147	2309±312	3617±364	5207±586
2QAN	480±79	786±133	1095±185	1435±259
Layered Sycamore				
<i>Entangling Gates</i>				
SABRE	157±11	394±24	687±35	1040±48
Tket	142±10	369±25	659±39	1002±60
2QAN	121±11	295±21	508±31	766±42
<i>Scaled Sched Time</i>				
SABRE	868±117	1603±225	2417±298	3267±424
Tket	918±114	1861±231	2793±289	3852±420
2QAN	428±79	653±115	879±140	1066±171
IBM’s Heavy Hex				
<i>Entangling Gates</i>				
SABRE	224±21	606±46	1095±62	1658±91
Tket	244±26	655±54	1188±82	1819±115
2QAN	172±19	450±38	817±58	1259±87
<i>Scaled Sched Time</i>				
SABRE	1259±183	2634±358	4017±472	5603±685
Tket	1395±170	2932±349	4756±508	6560±812
2QAN	603±118	1055±185	1478±245	1932±322
Rigetti’s Aspen				
<i>Entangling Gates</i>				
SABRE	206±22	578±45	1072±64	1681±90
Tket	202±15	635±48	1205±95	1967±106
2QAN	149±17	433±38	830±65	1307±72
<i>Scaled Sched Time</i>				
SABRE	1048±164	2198±307	3534±403	5052±659
Tket	1152±136	2720±295	4470±415	6810±631
2QAN	529±96	1025±185	1696±292	2400±392

TABLE IV
DATA AVERAGED OVER 100 RANDOMIZED PROBLEM INSTANCES OF WATTS STROGATZ (WS). VALUES ARE PRESENTED AS AVERAGE ± STANDARD DEVIATION.

may be made. For one, the ordering of lowest entangling gate count or smallest scaled scheduled time is not constant across problem instances. In fact, this list shifts significantly. The line architecture does not perform well in 12REG but does in Watts Strogatz and Sherrington-Kirkpatrick. This is interesting but may be understood from the fact that both the heavy hex and Aspen topologies are not much more than lines themselves with a few added connections. So, when the graph is dense enough the line architecture performs comparable to both commercial architectures.

Another interesting takeaway is that added complexity associated with non-planar coupling maps is not always worthwhile. For a fully connected graph the busNNN architecture outperforms all other architectures by a wide margin. However, for that same model the layered Sycamore chip and a generic 2D grid provide practically identical overheads. For the other two problem instances shown in Figure (12) the gap between busNNN and other architectures exists but is not significant in the regime of circuit widths shown. In these cases, using a simple 2D grid (which is easier to fabricate) would be acceptable. The main takeaway from these observations

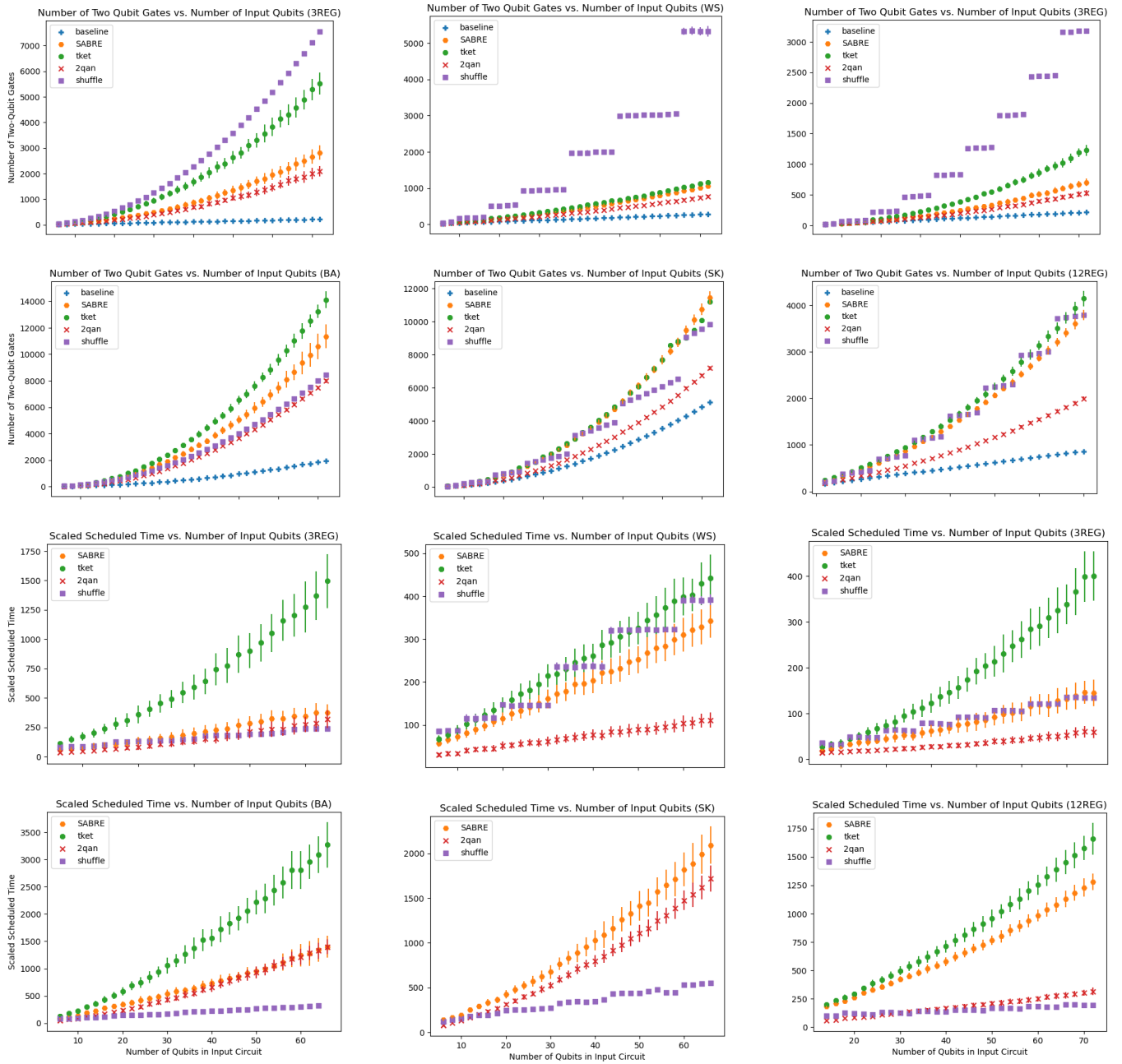


Fig. 9. The left column contains problem instances compiled on a line-type architecture. The middle and right are 2D grid and busNNN respectively. The type of problem instance is chosen to be representative of a wide variety of scaling. Tket is omitted from the bottom middle graph because its counts are so large that the rest of the data is obscured. Each graph contains data points for $6 \leq q \leq 72$ qubits

is that making blanket statements about one architecture’s utility versus another means very little without clarifying what problems one will be working with. Even in the context of 2-local Hamiltonians the variation between problem instances is nontrivial.

VI. CONCLUSION

It is clear that any design decisions considering coupling maps of superconducting NISQ architectures must be carefully weighed with data spanning compiling tools and problem instances. We have presented benchmarks of the performance

of various such tools across both coupling maps and problem instances we believe to be commercially and scientifically relevant. The newly proposed busNNN topology generally has the best performance in terms of the given metrics: entangling gate count and scaled scheduled time. Similarly, 2QAN consistently outperforms other heuristic compiling algorithms while the deterministic shuffle method of compilation outperforms all heuristics past some threshold connectivity and problem instance density. However, our benchmarking uses specific problem instances and gatesets. Future work can

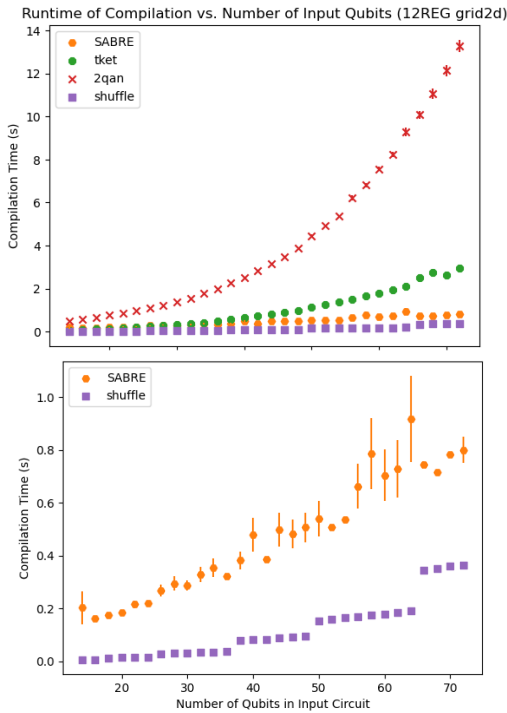


Fig. 10. Timing data measuring the compile time of each compilation tool. 2QAN quickly becomes unmanageable. The bottom graph omits 2QAN and Tket to make the scaling of SABRE and shuffle clear.

expand upon our choices and test other algorithms beyond 2-local Hamiltonians. This may require further research or even development of algorithms that can be run on NISQ hardware. It is an open question which algorithms make sense to run on near-term devices both in terms of size (width/depth) and competitiveness with classical algorithms.

Future work can also investigate how to bridge the performance gap of heuristic compiling algorithms in terms of our chosen metric and the scaling of deterministic compiling algorithms. Commutative SABRE has the option to shuffle an architecture to some desired mixing coefficient then apply SABRE to the resulting circuit. The impact of initial mapping on this strategy is not well understood. It is still possible to combine deterministic and heuristic algorithms in more clever ways; for example, to take advantage of the hierarchical nature of the busNNN architecture which we specifically designed to have a provably optimal swap strategy. Any progress towards lowering the overhead of compilation tools and their time scaling is a worthwhile pursuit.

The results presented in this study give evidence for utilizing QAOA (or recently optimized variations of QAOA) on certain problem graphs, on specific coupling maps compiled by distinct tools. The obvious goal of the work is to inform actual experiments on which choices to make in regards to architectures for superconducting NISQ devices. The methodology and tools developed for this work can be applied to new problem instances and architectures of interest in the future.

VII. ACKNOWLEDGMENT

We would like to thank Arthur Kurliej for his help with software development as well as previous work related to benchmarking hardware [29]. We thank John Blue for his insightful comments related to the swap strategy derived for the busNNN architecture.

REFERENCES

- [1] L. Ding, M. Hays, Y. Sung, B. Kannan, J. An, A. Paolo, A. Karamlou, T. Hazard, K. Azar, D. Kim, B. Niedzielski, A. Melville, M. Schwartz, J. Yoder, T. Orlando, S. Gustavsson, J. Grover, K. Serniak, and W. Oliver, "High-fidelity, frequency-flexible two-qubit fluxonium gates with a transmon coupler," *Physical Review X*, 2023.
- [2] Google Quantum AI, "Quantum supremacy using a programmable superconducting processor," *Nature*, 2019.
- [3] Y. Kim, A. Eddins, S. Anand, K. Wei, E. van den Berg, S. Rosenblatt, H. Nayfeh, Y. Wu, M. Zaletel, K. Temme, and A. Kandala, "Evidence for the utility of quantum computing before fault tolerance," *Nature*, 2023.
- [4] S. Herbert, "On the depth overhead incurred when running quantum algorithms on near-term quantum computers with limited qubit connectivity," *Quantum Information and Computation*, vol. 20, pp. 787–806, 08 2020.
- [5] A. Hagberg, P. Swart, and D. S. Chult, "Exploring network structure, dynamics, and function using networkx," tech. rep., Los Alamos National Lab.(LANL), Los Alamos, NM (United States), 2008.
- [6] A. Bestwick, "Introducing the ankaa-1 system - rigetti's most sophisticated chip architecture unlocks a promising path to narrow quantum advantage," 2023.
- [7] IBM Quantum, "The ibm quantum heavy hex lattice," 2021.
- [8] R. Stassi, M. Cirio, and F. Nori, "Scalable quantum computer with superconducting circuits in the ultrastrong coupling regime," *npj Quantum Information*, 2020.
- [9] B. marinelli, J. Luo, H. Ren, B. Niedzielski, D. Kim, R. Das, M. Schwartz, D. Santiago, and I. Siddiqi, "Dynamically reconfigurable photon exchange in a superconducting quantum processor," *PrePrint arXiv:2303.03507*, 2023.
- [10] A. Lucas, "Ising formulations of many np problems," *Frontiers in Physics*, vol. 2, 2014.
- [11] F. Glover, G. Kochenberger, R. Hennig, and Y. Du, "Quantum bridge analytics i: a tutorial on formulating and using qubo models," *Annals of Operations Research*, 2022.
- [12] B. Lodewijks, "Mapping np-hard and np-complete optimization problems to quadratic unconstrained binary optimization problems," *PrePrint arXiv:1911.08043v4*, 2020.
- [13] E. Farhi, J. Goldstone, and S. Gutmann, "A quantum approximate optimization algorithm," *PrePrint arXiv:1411.4028*, 2014.
- [14] E. Farhi, J. Goldstone, and S. Gutmann, "A quantum approximate optimization algorithm applied to a bounded occurrence constraint problem," *PrePrint arXiv:1412.6062v2*, 2015.
- [15] E. Fahri and A. Harrow, "Quantum supremacy through the quantum approximate optimization algorithm," *PrePrint arXiv:1602.07674v2*, 2019.
- [16] B. Korte and J. Vygen, *Combinatorial Optimization Theory and Algorithms*. Springer-Verlag Berlin Heidelberg, 2000.
- [17] M. Dupont and B. Sundar, "Quantum relax-and-round algorithm for combinatorial optimization," *PrePrint arXiv:2307.05821*, 2023.
- [18] J. Finžgar, A. Kerschbaumer, M. Schuetz, C. Mendl, and H. Katzgraber, "Quantum-informed recursive optimization algorithms," *PrePrint arXiv:2308.13607*, 2023.
- [19] G. Li, Y. Ding, and Y. Xie, "Tackling the qubit mapping problem for nisq-era quantum devices," in *Proceedings for the International Conference on Architectural Support for Programming Languages and Operating Systems*, pp. 1001–1014, Association for Computing Machinery, 2019.
- [20] A. Cowtan, S. Dilkes, R. Duncan, A. Krajenbrink, W. Simmons, and S. Sivarajah, "On the qubit routing problem," in *Leibniz International Proceedings in Informatics*, 2019.
- [21] L. Lao and D. Browne, "2qan: a quantum compiler for 2-local qubit hamiltonian simulation algorithms," in *Proceedings for International Symposium for Computer Architecture*, Association for Computing Machinery, 2022.

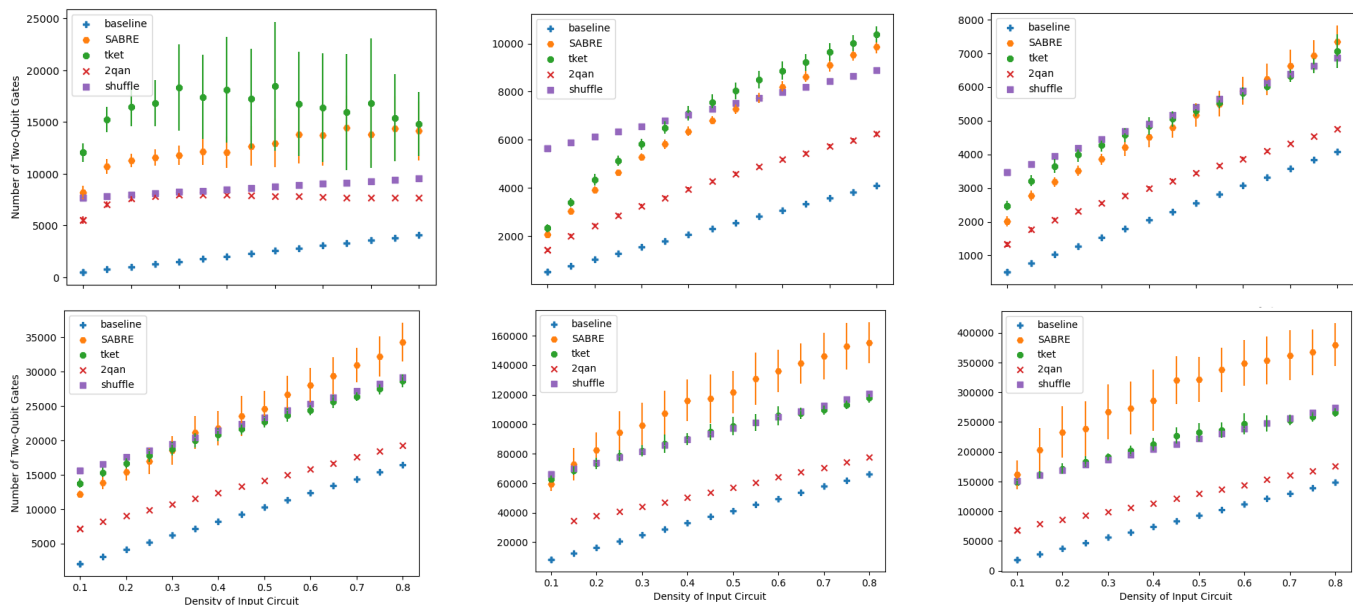


Fig. 11. How entangling gate count scales with problem instance density for random graphs. From left to right, the top row depicts the line, grid, and busNNN topologies all with circuit width $n = 72$. The bottom row depicts the busNNN architecture with $n = 144, 288, 432$ qubits from left to right.

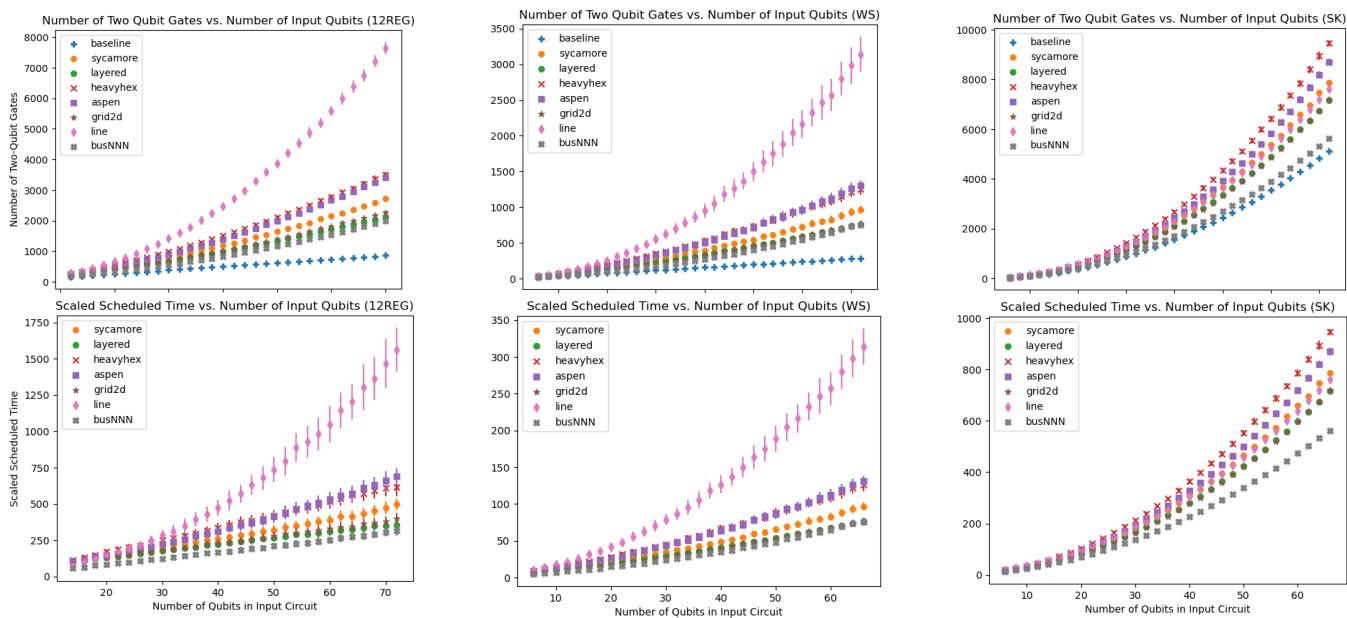


Fig. 12. Comparison of all architectures, using the best compiler for each. From left to right we have 12REG, WS, and SK problem instances. The top row has two qubit gates as the chosen metric and the bottom row is using scaled scheduled time.

[22] J. Liu, L. Bello, and H. Zhou, “Relaxed peephole optimization: a novel compiler optimization for quantum circuits,” in *International Symposium on Code Generation and Optimization*, IEEE Association for Computing Machinery, 2021.

[23] L. Sauras-Altuzarra and E. Weisstein, “Adjacency matrix,” 2023.

[24] M. Gendreau and J.-Y. Potvin, *Tabu Search*, pp. 165–186. Boston, MA: Springer US, 2005.

[25] Y. Jin, J. Luo, L. Fong, Y. Chen, A. Hayes, C. Zhang, F. Hua, and E. Zhang, “A structured method for compiling and optimizing qaoa circuits in quantum computing,” *PrePrint arXiv:2112.06143*, 2022.

[26] J. Weidenfeller, L. Valor, J. Gacon, C. Tornow, L. Bello, S. Woerner, and D. Egger, “Scaling of the quantum approximate optimization algorithm on superconducting qubit based hardware,” *Quantum*, 2022.

[27] M. Nielsen and I. Chuang, *Quantum Computation and Quantum Information*. Cambridge University Press, 2000.

[28] A. Reuther, J. Kepner, C. Byun, S. Samsi, W. Arcand, D. Bestor, B. Bergeron, V. Gadepally, M. Houle, M. Hubbell, M. Jones, A. Klein, L. Milechin, J. Mullen, A. Prout, A. Rosa, C. Yee, and P. Michaleas, “Interactive supercomputing on 40,000 cores for machine learning and data analysis,” in *2018 IEEE High Performance Extreme Computing Conference (HPEC)*, pp. 1–6, IEEE, 2018.

[29] A. Kurler, S. Alterman, and K. Obenland, “Benchmarking and analysis of noisy intermediate-scale trapped ion quantum computing architectures,” *IEEE International Conference on Quantum Computing and Engineering*, 2022.